Inherited control of crystal surface reactivity

Fischer, C.; Kurganskaya, I.; Lüttge, A.;

Originally published:

February 2018

Applied Geochemistry 91(2018), 140-148

DOI: https://doi.org/10.1016/j.apgeochem.2018.02.003

Perma-Link to Publication Repository of HZDR:

https://www.hzdr.de/publications/Publ-26582

Inherited control of crystal surface reactivity

Cornelius Fischer[1]*, Inna Kurganskaya[2], and Andreas Luttge[3,4]

[1]Helmholtz-Zentrum Dresden-Rossendorf, Inst. f. Ressourcenökologie, Abt. Reaktiver Transport, Permoserstr. 15, D-04318 Leipzig, Germany;

[2]Institute of Geological Sciences, University of Bern, Baltzerstrasse 3, Bern 3012, Switzerland

[3]MARUM & Fachbereich Geowissenschaften, Universität Bremen, D-28359 Bremen, Germany;

[4]Department of Earth Science, Rice University, Houston, TX 77005, USA

*corresponding author: c.fischer@hzdr.de

Abstract: Material and environmental sciences have a keen interest in the correct prediction of material release as a result of fluid-solid interaction. For crystalline materials, surface reactivity exerts fundamental control on dissolution reactions; however, it is continuously changing during reactions and governs the dynamics of porosity evolution. Thus, surface area and topography data are required as input parameters in reactive transport models that deal with challenges such as corrosion, CO_2 sequestration, and extraction of thermal energy. Consequently, the analysis of surface reaction kinetics and material release is a key to understanding the evolution of dissolution-driven surface roughness and topography. Kinetic Monte Carlo (KMC) methods simulate such dynamic systems. Here we apply these techniques to study the evolution of reaction rates and surface topography in crystalline materials. The model system consists of domains with alternating reactivity, implemented by low vs. high defect densities.

Our results indicate complex and dynamic feedbacks between domains of high versus low defect density, with the latter apparently limiting the overall dissolution rate of the former - a limitation that prevails even after their disappearance. We introduce the concept of "inherited" control, consistent with our observation that maximum dissolution rates in high defect density domains are lower than they would be in the absence of low defect density neighboring domains.

The controlling factor is the spatial pattern of surface accessibility of fluids. Thus, the distribution of large etch pits centers is inherited almost independently of spatial contrasts in crystal defect density during ongoing reactions. As a critical consequence, the prediction of both the material flux from the reacting surface and the evolution of topography patterns in crystalline material is constrained by the

reaction history. Important applications include the controlled inhibition of reactivity of crystalline materials as well as the quantitative evaluation and prediction of material failure in corrosive environments.

Keywords: Kinetic Monte Carlo simulation, rate spectra, crystal dissolution, surface reactivity, surface topography and roughness patterns

1 Introduction

Crystal defects cause the formation of etch pits during dissolution and corrosion processes. A large body of literature exists about this process, ranging from BCF theory to the stepwave model (e.g., Casey et al., 1988; Cheng, 1993; Dove et al., 2005; Lasaga and Luttge, 2001; Luttge et al., 2013; Tang et al., 2003). The growth and coalescence of etch pits controls the evolution of reacting rough surfaces and pore walls and affects thus porosity in natural and technical materials. Examples include the formation of secondary porosity in reservoirs (Taylor et al., 2010) or the impact of microstructures on corrosion (Horlait et al., 2014). As a consequence, small-scale approaches for modeling pore-scale reaction processes are gaining increased interest (Iliev et al., 2015; Steefel et al., 2015). The evolution of porosity alters the fluid-solid interface and, thus, the effective reactivity of the dissolving material (Daval et al., 2013; Dele-Afolabi et al.; Dong et al., 2011; Fischer et al., 2014; Xu et al., 2016). By changing the surface roughness and topography of the reacting pore walls and throats (Anbeek, 1992), the evolution of new void volumes constrains via permeability alternations both the diffusive and advective transport of dissolved material and thus impacts reactive flow conditions (Anovitz and Cole, 2015; Gao et al., 2017; Iliev et al., 2015; Mostaghimi et al., 2016). Moreover, coupled dissolution–precipitation reactions rely on the formation of voids as initial pore volumes as this allows the fluid to maintain contact with the reacting interfaces (Chen et al., 2014). Accordingly, the quantitative predictability of porosity evolution during fluid-solid interaction is of great interest in multiple disciplines of material and environmental sciences, and the development of appropriate tools is at the forefront of fundamental and applied research (Steefel et al., 2015; Yang et al., 2015). The formation of void volumes significantly influences the efficiency of fluid-solid interactions by affecting the rate of solute transport. Related data are required as input parameters in reactive transport models dealing with questions such as CO_2

sequestration (Hellevang et al., 2013; Monger et al., 2015), extraction of thermal energy (Dillinger et al., 2014), as well as waste management in rock formations (Kim et al., 2011).

Crystal surface reactivity is an important but variable boundary condition that constrains the evolution of porosity. The defect density variability in crystalline materials is a critical parameter that defines spatial domains of contrasting reactivity (Hiemstra and van Riemsdijk, 1999). The accessibility of domains with constant or contrasting surface reactivity does change continuously over reaction time. Thus, changing surface-energetic complexity does superimpose the changing geometric complexity. As a consequence, the boundary conditions of the reacting system change dynamically. The analysis of such a system with multiple changing input parameters is a classic task for a modelling approach. Kinetic Monte Carlo (KMC) simulation calculations offer a large enough length scale to address this problem appropriately (Lasaga and Blum, 1986).

As a starting point, we study the evolution of reaction rates and surface topography pattern in a simple *Kossel* crystal (Kossel, 1927; Stranski, 1928) by utilizing KMC simulation techniques. More specifically, the model material is built up of domains of constant activation energies but having varying defect densities in order to provide well-defined variations in the surface reactivity (Liu et al., 2017; Liu et al., 2015; Luttge et al., 2013). We apply the rate spectra concept to KMC results in order to analyze systematically the rate contributors in the frequency domain of rate datasets (Fischer et al., 2012; Fischer et al., 2014). Using this concept, the identification of both invariance or temporal variability of such rate contributors over reaction time provides quantitative insight into the overall reaction rates of crystalline materials (Fischer and Luttge, 2017; Michaelis et al., 2017; Saldi et al., 2017).

In detail this study addresses the following questions: (1) How variable are reaction rates during dissolution of multiple domains or grains of crystalline material with variable defect density? Do such domains provide constraints to the effective surface reactivity? (2) How variable are the resulting pore volume and etch pit distribution? What parameters govern the initial formation of topography patterns in crystalline material? Is there any predictive power associated with such a parameter? (3) To what extent is reactivity inherited in crystalline material? Are low-reactivity domains able to slow down the overall reaction rate significantly with consequences such as reduction in surface reactivity?

2 Methods

2.1 Kinetic Monte Carlo simulations

A Kinetic Monte Carlo (KMC) program simulates a series of single reactions at the atomic scale. Here, we apply a KMC model for a *Kossel* crystal (Kossel, 1927). A Kossel crystal consists of a cubic lattice composed of a single chemical species. The bond energies Φ between all atoms are constant. The KMC model is based on the Bortz-Kalos-Lebowitz (BKL) algorithm (Bortz et al., 1975). The algorithm allows for a reactive event at each iteration step. The simulation provides the temporal evolution of a dissolving surface, based on a series of single reaction events on the crystal surface. Lasaga and Luttge (2004) provide detailed and general information about KMC models for mineral dissolution. In this study, the model simulates dissolution reactions under conditions far from equilibrium.

KMC models are now routinely used for studying surface site-specific reaction kinetics (e.g., Cama et al., 2010; Kerisit et al., 2008; Kurganskaya and Luttge, 2016; Meakin and Rosso, 2008). Implemented parameters in KMC algorithms include the lattice resistance effect or the network of surface hydrogen bonds. An increasing number of ab initio calculations provides the critical parameters for the probability equations. Thus, the reactivity of solid materials without defects is properly implemented in KMC approaches. In this study, we focus on the impact of varying defect densities in crystals. The reported variability in natural and technical crystalline material is huge and includes several orders of magnitude (Blum and Lasaga, 1987), similar to the ranges utilized in this study (**Table 1**).

We utilize periodic boundary conditions to eliminate the influence of model size in (x,y) direction. In order to investigate material domains of varying reactivity, we apply a “layered cake” model of a solid, composed of layers with variable thickness and defect densities. The type of crystal defects in this study are screw dislocations. Screw dislocations form an initial structure during the dissolution process, i.e., the hollow core. Ongoing dissolution results in the formation of etch pits along the hollow core. Our model has well-defined input parameters, i.e., the number of layers, layer thickness, and defect density (**Table 1**). Defects are randomly seeded in each layer by using uniformly distributed random numbers for (x,y) core center positions. The defect length is identical to the domain thickness.

Table 1: KMC simulation parameters for the dissolution of KOSSEL crystals with a lattice constant of 0.2 nm. Several KMC runs utilized crystals that are built-up of several domains in z-direction (domain thickness) that are characterized by alternating defect densities. In this case, a structure starting with a high (*h*) reactivity domain followed by a low (*l*) reactivity domain was analyzed and vice versa, e.g., *hlhl* & *lhlh*, see **Fig. 2**.

Simulation results in	**system size (area)**	**domain thickness**	**defects/ domain**	**number of domains**	**dissolved atoms**	**number of runs**
Fig. 1	50×50 nm^2	10 nm	50	1	1E+06	1
Figs. 2, 3	300×300 nm^2	1 nm	1000 (*h*) 10 (*l*)	4	1E+06	2
Fig. 3C	300×300 nm^2	10 nm	1000	1	1E+06	1
			100	1	1E+06	1
			10	1	1E+06	1
Figs. 4, 5	300×300 nm^2	10 nm	150 (*h*) 15 (*l*)	2	10E+06	2
Fig. 6	300×300 nm^2	2 nm	100 (*h*) 10 (*l*)	10	6E+06	2
Fig. 7	300×300 nm^2	20 nm	100 (*l*)	1	6E+06	1
		2.0 nm	100 vs. 10	10		
		2.2 nm	110 vs. 11	10		
		4.0 nm	200 vs. 20	10		
		20 nm	1000 (*h*)	1		

The simulation starts with the opening of hollow cores in the top layer. As soon as the dissolving layer exposes a defect outcrop in the subjacent layer, a hollow core opens and a new etch pit evolves (Burton et al., 1951; Lasaga and Luttge, 2001). KMC runs were performed under constant bond strength conditions ($\Phi = 4$, normalized to kT units). The dissolution probability P_i of an atom with i bonds is

$$P_i = e^{\left(-\frac{\Phi}{kT}\right)} \quad (1)$$

Multiple types of reactive domains were used in layered cake models. We investigated the impact of defect density and domain thickness in different KMC simulation calculations, details about the parameter variation of the crystals are summarized in **Table 1**. We varied the starting conditions of the model, i.e., the reactivity of the uppermost layer was either (*h*) or (*l*).

2.2 Reaction rate analysis: rate maps and rate spectra

Rate maps are calculated using the formula:

$$R(x, y, t_i) = \frac{h(x,y,t_{i-1}) - h(x,y,t_i)}{t_i - t_{i-1}} = \frac{\Delta h_i(x,y)}{\Delta t_i} \quad (2)$$

130 R (x,y,t) is the local dissolution rate for a single node, defined by (x,y) coordinates, and i is the time
131 step. Such rates reflect the increase (growth) or decrease (dissolution) of the initial height h of a given
132 point (x,y) during a time interval ($t_i - t_{i-1}$). The frequency distribution of the R values forms a rate
133 spectrum (Fischer et al., 2012). The simulations output the surface height maps at fixed iteration steps,
134 the distributions of the reactive sites, and the overall material flux as a function of time. The iteration
135 steps are defined by the number of dissolved blocks. The reaction time increment, Δt_i, between the
136 events $i-1$ and i, is calculated as a reciprocal sum of the number N of probabilities P of surface
137 reactions normalized by the reaction attempt frequency, v (Blum and Lasaga, 1987), i.e., the
138 fundamental frequency (Pelmenschikov et al., 2001), that we set to 10^{12} [s^{-1}]:

139 $$\Delta t_i = \frac{1}{v \sum_{j=1}^{N} P_j} \quad (3)$$

140 This permits the tracking of the reaction progress and to analyze kinetic parameters such as overall rate,
141 kink and step site densities in time units (TU, see below). The applied fundamental frequency number
142 is in the order of magnitude of the intermolecular vibrational frequency of bulk water (Walrafen, 1972).
143 The frequency of the reaction attempts is similar to this frequency because the dissolution process is
144 water-catalyzed (Pelmenschikov et al., 2001). Consequently, bond strengths are utilized for probability
145 calculations.
146

3 Results and discussion

3.1 Quantitative analysis of surface reaction rates

Material flux maps provide information about the spatial distribution of heterogeneous material flux. Flux maps of KMC calculation results offer the opportunity to analyze the mechanistic connection between crystal surface reactions and material flux at any time step. **Figure 1** exemplifies how this analysis reveals information about material flux characteristics.

Based on KMC results, a model for crystal dissolution via the stepwave movement mechanism has been introduced (Lasaga and Luttge, 2001). According to this model, crystal dissolution is controlled by stepwaves emanating from dislocation cores (**Fig. 1A; B**). The evolution of superimposing stepwaves and their efficiency in terms of material removal is quantitatively illustrated by using material flux maps (**Fig. 1C**) and the corresponding rate components **(Fig. 1D**).

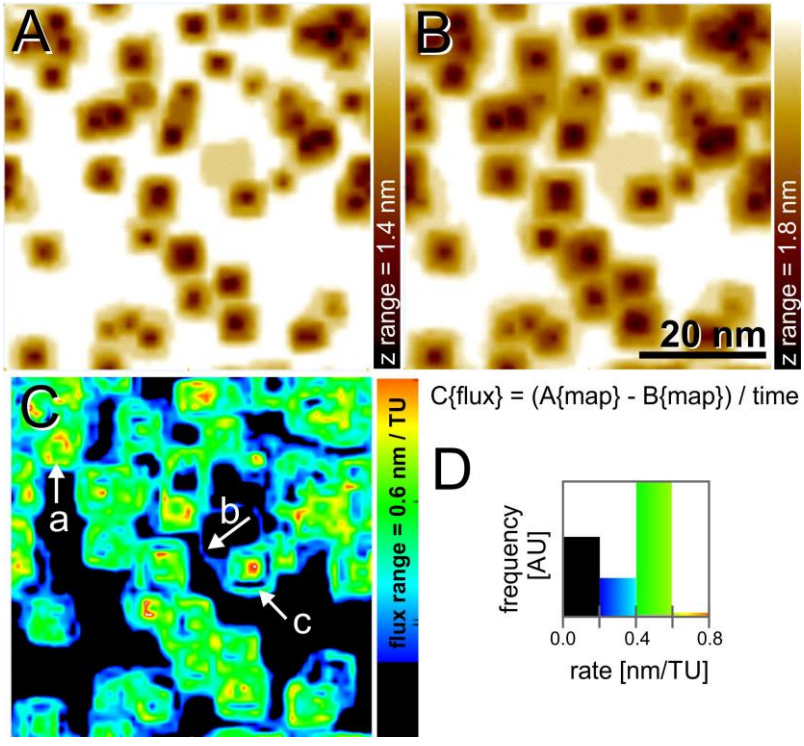

Figure 1: Visualization of results of a Kinetic Monte Carlo dissolution experiment using a *KOSSEL* crystal structure. (A, B) Topography with etch pits after removal of 100'000 and 200'000 blocks. (C) Material flux map shows inert (black) and reactive surface sections related to surface rates. Note the distribution and shape of reactive surface portions: a. highly reactive etch pit wall sections (yellow/red), b. single stepwave of an extinct screw dislocation, c. flux distribution related to complex stepwave structure with change of surface reactivity at an etch pit wall. (D) Rate spectrum of rate map (C) showing the dominant frequency (green color) of rate contributions owing to dissolution stepwaves.

As an example, large single stepwaves from inactive screw dislocations (at the height of screw bottoms) represent low material fluxes. Superimposition of stepwaves from multiple generators results in flux map sections that illustrate a complex pattern of high vs. low material flux distribution.

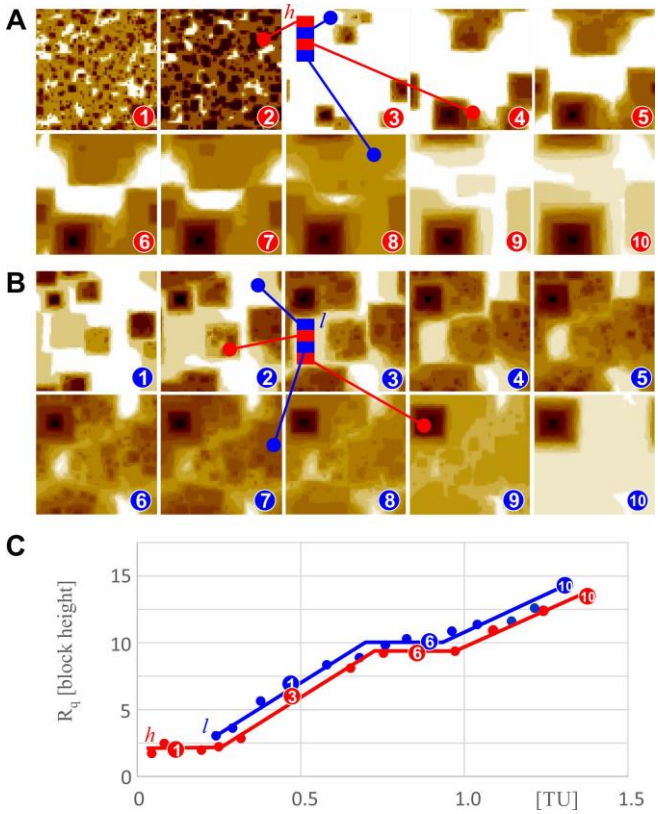

Figure 2: (A) Surface topography evolution of a KOSSEL crystal that consists of four layered domains having alternating defect densities, starting with a high defect density (1000 defects/domain), followed by a low defect density (10 defects/domain). (B) Topography evolution similar to (A), but starting with a low defect density (10 defects/domain), followed by a high defect density (1000 defects/domain). The column sketches in (A) and (B) illustrate the impact of the contrasting defect densities (low (*l*): blue; high (*h*): red) on etch pit size and number. (C) Evolution of RMS roughness *Rq* of both materials (A) and (B). Map size = 300 × 300 nm^2. Note the difference in reaction time compared to the dissolution of an identical number of surface blocks, e.g. (1)-red vs. (1)-blue due to initial differences in surface reactivity (see A, B).

3.2 Reactivity of layered crystals with domains having varying defect densities

We compare the dissolution rates of KOSSEL crystals that are composed of domains of contrasting screw defect densities. We vary the initial conditions with respect to the defect density of the uppermost crystal domain, i.e., high (*h*) vs. low (*l*) reactivity (**Table 1**). **Figure 2** illustrates the evolution of the surface topography and roughness (**Fig. 2 A**: *h*, **B**: *l*). As expected, the initial topographic contrast of the surface maps of both crystals is caused by the defect density (Anbeek et al., 1994). A high defect

density results in the formation of multiple etch pits having a small lateral extension (**Fig. 2A**, 1-2), a low defect density results in the formation of a few pits with large lateral size (**Fig. 2B**, 1). Subsequently, the dissolution of the subjacent crystal domain leads to the superimposition of small and large etch pits, according to the defect density of the newly-exposed crystal domains. However, the roughness evolution (**Fig. 2C**) is dominated by the topography of large and deep etch pits. The change in-between low- vs. high-reactivity has no clear equivalent in the topography evolution. The reason is that the evolution and growth of a few large pits is a dominant factor of the overall evolution of surface topography. Consequently, the RMS roughness (Thomas, 1999) increases over the total reaction time.

Figure 3 shows the rate maps of the dissolving crystalline material. **Figure 3A** illustrates the locally low rates associated with the dissolution of material having a high defect density (**Fig. 3A**, [1-2], blue color). The growth of etch pits within crystal domains with low defect densities results in locally enhanced reaction rates (**Fig. 3A**, [4], green color). The existence of steep etch pit walls (**Fig. 2**) dictates the further evolution of surface rates and topography, i.e., the increase in spatial heterogeneity of material flux from the surface. A similar evolution is observed for crystal domains with an inverse order of defect density (**Fig. 3B**). The initial contrast in surface rates of high vs. low defect density domains is clearly visible in **Fig. 3C**, sections [1-2] of both *h* and *l* domains. The large initial contrast of the material flux is decreased irreversibly during the ongoing reaction, see **Fig. 3C**, all map sections later than [2]. For comparison, **Fig. 3C** shows the rate evolution during dissolution of KOSSEL crystals with constant defect densities (10, 100, 1000 defects/unit volume). The initial results of the material release s are similar to the above investigations, see **Fig. 3C**, sections 1-2 of both *h* and *l* domains and homogeneous crystals with high (1000) and low (10) defect densities. However, the subsequent rate evolution of both layered crystals is similar to those of the homogenous crystal with the lowest defect density (blue dotted line in **Fig. 3C**). Thus, we hypothesize that crystal domains with low defect densities act as inhibitors. Below, we investigate this point in greater detail.

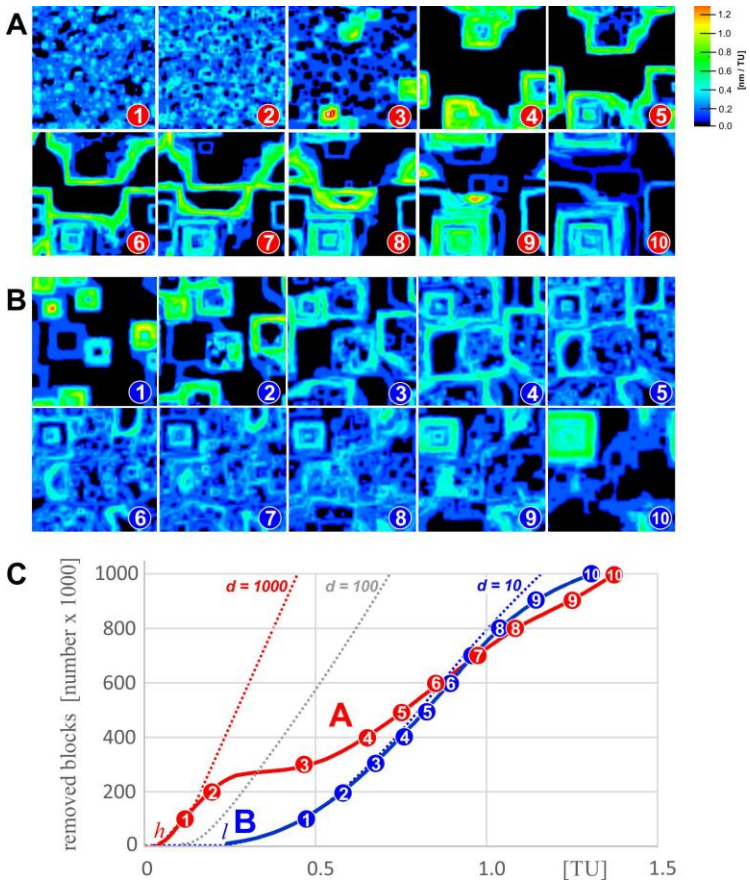

Figure 3: Surface rate evolution of the KOSSEL crystal shown in **Fig. 2**. (A) Rate maps resulting from the dissolution of four layered domains having alternating defect densities, starting with a high defect density (1000 defects/domain), followed by a low defect density (10 defects/domain). (B) Surface rate evolution similar to (A), but starting with a low defect density (10 defects/domain), followed by a high defect density (1000 defects/domain). (C) Evolution of the rate [expressed by total number of removed blocks] of both materials (A) and (B). For comparison, simulation results are shown of single domains having 1000, 100, and 10 defects, respectively. Map size = 300 × 300 nm^2.

3.3 Rate spectra analysis of reaction inhibition

We analyzed rate spectra in order to investigate the relationship between reaction kinetics, surface topography, and potential inhibition of surface reactivity. **Figure 4** illustrates the surface evolution (**Fig. 4A-D**) and the respective rate spectra (**Fig. 4A'-D'**). During dissolution of the upper crystal domain, the evolution of both surface topography and rate spectra reflects the situations of low defect density (**Fig. 4A, A'**) vs. high defect density (**Fig. 4C, C'**), cf. **Table 1**. Both rate spectra show an asymmetric shape. The less reactive crystal domain is characterized by a spectrum with a tail towards lower rate components. Accordingly, the more reactive crystal domain shows the opposite behavior. Then, the underlying domain gets partly and later completely exposed to dissolution during the ongoing removal of the upper domain. **Figures 4B, D** illustrate the crystal surface topography after complete removal of

the uppermost domain. At this time, both surfaces are dominated by large etch pit structures. It is a surprising result that the high defect density of the newly exposed material in **Figure 4 B** does not impact significantly the reaction rate.

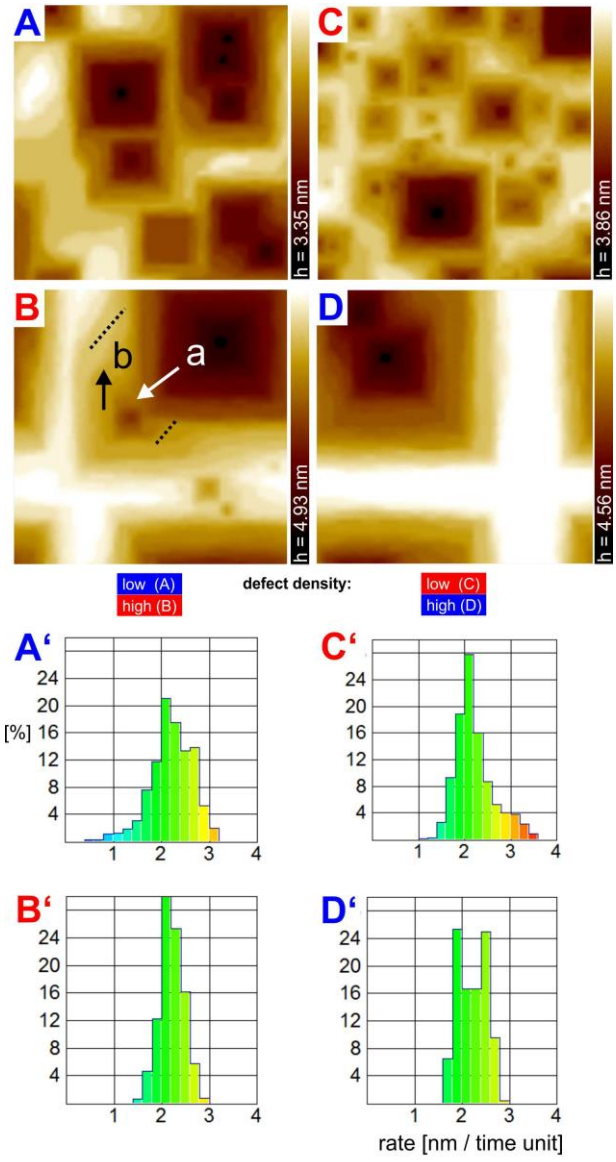

Figure 4: Surface topography and rate spectra evolution of two different layered cake model structures. Left (A,B) with low (blue, upper part) and high (red, lower part) reactivity domains (dt = 5×10^9 s). Right (C,D) shows inverse order of domain reactivity (dt = 6×10^9 s). Corresponding rate spectra (A', B') and (C', D') are shown below, time unit (TU) = 6×10^9 s. System size = 300×300 nm^2.

Etch pits related to the high defect densities do open and their frequent occurrence is visible at the walls of the large pit structure. Their spatial evolution is geometrically constrained and hindered by the large pit structure which produces surface steps much faster than the newly-formed pits. Both the lifetime of pits and their impact on the overall rate are thus restricted by the final stepwave velocity dictated by the

large pit (Lasaga and Luttge, 2001). This result is illustrated by the characteristic shape of the rate spectrum (**Fig. 4B'**). Here, the expected asymmetric shape towards higher rates (cf. **Fig. 4 C'**) is not observed. Instead, the rate spectra shapes of contrasting domains are fairly similar (**Figs. 4 B' and D'**). This result shows that the initial low surface reactivity and the corresponding surface evolution are able to constrain the effective reactivity of a material at later development stages, regardless of its defect density. Thus, a proxy such as defect density is not in general able to serve as an input value for the prediction of reactivity and material flux. Based on defect density we would expect a change to higher material flux and thus a higher reaction rate (**Fig. 4 B, B'**). The rate spectra analysis, however, does show that the expected elevated reactivity of the material is limited due to the previous reaction steps.

3.4 Evolution of material flux and surface topography

We investigate the evolution of an important reactive crystal surface site density, i.e., kink sites, and compare their frequency with the evolution of the cumulative material flux (overall void volume) and the rough topography of the reacting surface. In **Figure 5**, the transition between domains of contrasting reactivity is indicated by pairs of dashed lines.

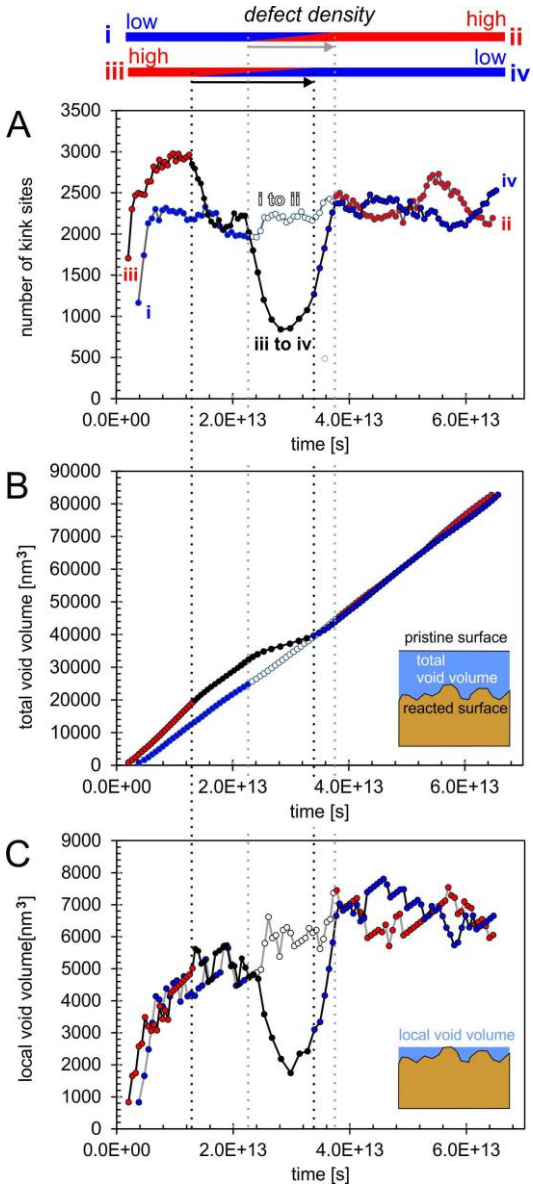

Figure 5: (A) evolution of kink site number, (B) evolution of total dissolved volume, (C) evolution of local void volume (related to rough surface topography) in two different settings (black line, initially high reactivity, gray line: initially low reactivity). Blue and red letters refer to the reactivity of crystal domains, see Fig. 2. Pairs of dashed lines refer to the interface between domains of contrasting reactivity, i.e., initial exposition of underlying domain and complete removal of upper domain.

This transition represents the reaction period that starts with the initial exposure of material from the underlying domain and ends with the complete dissolution of material from the upper domain. The contrast in reactivity of the upper domains in both systems (low – i vs. high – iii) is illustrated by the contrast of surface kink site concentration during the initial reaction period (**Fig. 5 A**). Thus, the material flux from the more reactive domain with higher defect density is higher (red vs. blue circles). While the void volume formation and the kink site density during this reaction period are not identical, the void volumes of the rough topographies are similar (**Fig. 5**).

This picture changes during the reaction period that is required to remove the material of the upper domain completely. The concentration of kink sites of the highly-reactive domain drops significantly (red → black circles; iii→iv). This is caused by the high consumption rate of the material of the highly-reactive domain and synchronously the low rate of etch pit and kink site formation in the underlying low-reactivity domain. Consequently, the cumulative material flux decelerates (**Fig. 5 B**) and the corresponding surface pore volume (**Fig. 5 C**) shows a minimum value. One would expect that this picture does reverse after the complete removal of the upper domain of the initially low-reactive crystal (blue → open circles; i→ii). However, the interesting result is that both the kink site density and the overall material flux of the highly reactive domain (**Figure 5**: open symbols) do not mirror the picture that we observed initially. Instead, the kink site density of both experiments (**Fig. 5 A**, right section) fluctuates around a mean value similar for both systems. Some fluctuations during the dissolution period of the crystal domain with higher defect density (see section (ii)) are caused by an undisturbed growth of newly-formed etch pits. A similar behavior is observed for the void volumes (**Fig. 5 B,C**). These results explain the observations of the limited reaction rates that are illustrated in **Figure 4 B & 4 B'**, see above. Our interpretation is as follows: While the defect density of the highly-reactive domain supports the frequent opening of pits, the life-time of their stepwaves is comparatively short. Consequently, the reactivity of the system is no longer defined by its defect density but rather by the existence of inherited etch pit positions and their large size compared to newly-formed pits (**Fig. 4B**). The position of such pits has been inherited from the previously dissolving domain because the bottom of such deep pits provide the initial exposure to the subjacent crystal domain. As soon as a surface section of the latter had been exposed, the seeding of a new pit started because of the high probability of exposing a defect and opening of a hollow core.

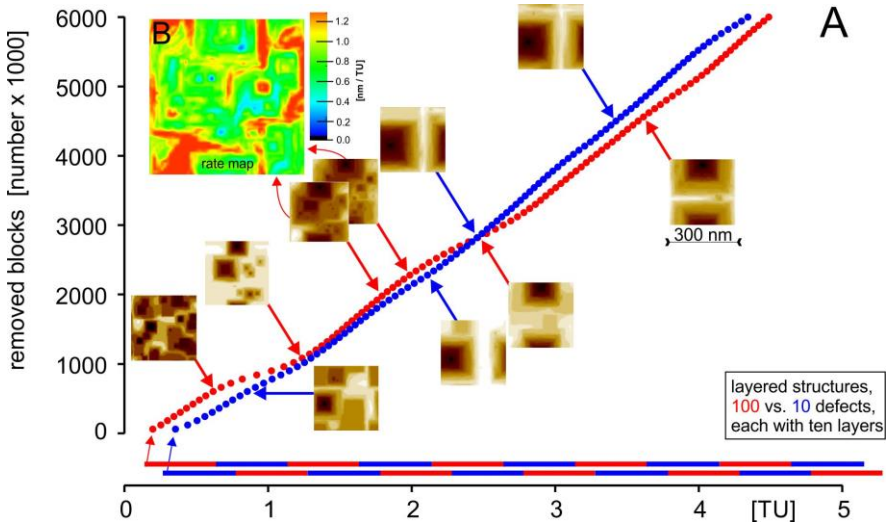

Figure 6: (A) Temporal variability of the material flux of dissolving KOSSEL crystals with 10 domains having alternating reactivity, implemented by the number of defects per domain (10 vs. 1000). The blue-colored curve indicates results of a crystal starting with a low-reactivity domain, the red-colored curve represents a crystals having a high-reactivity starting domain. Topography maps (amber-colored) illustrate the respective topographies. (B) Rate map (topography difference map based on topography maps (38 – 33) identifies large etch pit walls as the source of highest rate portions.

3.5 Analysis of larger systems

The results in **Figs. 3 and 4** suggest the inhibition of surface reactivity by crystal domains with low reactivity. In this subchapter we ask the question whether this result is valid during the long-term evolution of dissolution of multiple crystal domains (e.g., Taleb and Stafiej, 2011). We investigate such behavior by using KOSSEL crystals that consist of a larger number layered domains (**Table 1**). **Figure 6** shows the results of the long-term simulations using a system that consists of 10 layers. Here, the initial sections of the rate curves show the expected contrast, i.e., a higher number of removed blocks of the highly-reactive surface portion compared to the low reactivity material at the identical time step, see also **Figure 3C**. Subsequently, both rate curves indicate results that are typical for systems with low surface reactivity and, thus, low reaction rates. Similar to the shorter simulation runs (**Figs. 2-5**), the reactivity of the dissolving crystal is dictated by the low-reactivity domains. The surface maps of both systems explain such behavior (**Fig. 6**). The long-term evolution of the reacting crystal surfaces is characterized by the evolution of large single pits. This typical result illustrates the dominant growth of large pits on the expense of small pits. Regardless of the opening of new etch pits, the further growth of existing large pits is the dominating process (**Fig. 6B**).

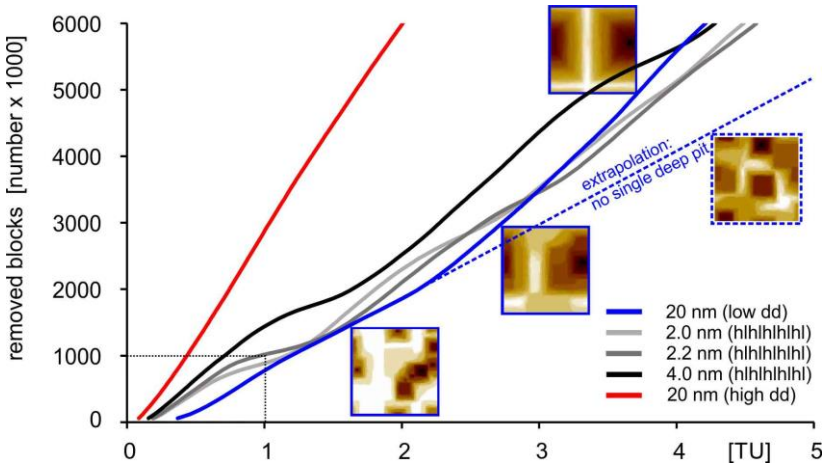

Figure 7: (A) Long-term rate evolution as a function of domain thickness. Three domain thicknesses (2.0, 2.2, 4.0 nm with alternating defect density high vs. low) are investigated. Low (blue) and high (red) defect density (dd) domains are shown for comparison. The dotted line represents a shorter reaction period similar to those analyzed in Figure 3.

The results in **Figure 7** illustrate the impact of varying domain thickness on the overall reactivity and material flux during dissolution. The grey-colored lines represent different thicknesses of the alternating domains (**Table 1**). We compare the results with systems having constant defect densities. Overall, the reduction in reactivity of the crystals having domains of contrasting defect density is found again, similar to observations of alloy corrosion (Renner et al., 2006). Our results suggest a complex impact of the domain thickness on the dissolution of a series of domains. The change of domain thicknesses causes a non-linear change in reactivity and rates of the compound. Accordingly, both slope and position of inflection points suggest a complex interplay in-between defect density/ etch pit number, domain thickness, and material flux/ reaction rate. As an example, the crystal with domain thicknesses = 4.0 nm shows a higher rate compared to the other examples (2.0 nm and 2.2 nm). Nevertheless, the elevated reactivity that is represented by the crystal without any domains is not reached during the entire reaction period. Moreover, the reactivity of this crystal (d = 4.0 nm) having high-reactivity domains drops temporarily below the reactivity of the low-defect density crystal. Geometrical constraints related to the evolution of rough surface topography during the etch pit growth are a potential explanation.

Figure 7 illustrates another important characteristics of any reacting crystal, exemplified by the blue-colored rate curve. During the comparatively long reaction period, the reaction rate increases as shown by the deviation from the dashed line. Such behavior can be explained by the occurrence of large etch

pit walls having high kink site densities as the major portion of the overall crystal surface. Similar results have been reported for the dissolution reaction of grains of single crystals (Briese et al., 2017; Petrik and Harbrecht, 2013). Thus, an additional important parameter that exerts control on the system's reactivity is the domain size and the related opportunity to form large etch pits with a characteristic high surface roughness and topography.

Previous attempts to quantify the surface rates vs. etch pit nucleation focused on pit size distribution analysis (MacInnis and Brantley, 1993). Such approaches compared the varying size, distribution, and coalescence of pits with reaction rates of single crystal surfaces (Luttge, 2005). Experimental approaches showed how spatial heterogeneities in both surface kinetics and material transport properties evolve during single crystal dissolution (Peruffo et al., 2013). As a result, the morphology of the characteristic etch features may reveal direction-dependent dissolution kinetics. Our approach utilizes this knowledge and applies it to more complex model systems in order to extract important new information about the evolution of reactivity. More specifically, the temporal evolution of rate spectra informs about material flux variability and relates it to etch pit formation, growth, and coalescence (Fischer and Luttge, 2017). Rate acceleration and rate jerk data suggested the pulsating behavior of surface reactivity (Fischer and Luttge, 2018). Overall, the modeling results focusing on varying defect density underscore the critical role of reactivity anisotropy in crystalline material for the evolution of surface roughness and void volume pattern due to dissolution. More specifically, these results show how the spatial distribution of high vs. low reactivity domains in crystal grains impacts the evolution of void volume patterns in materials that are characterized by an identical mean defect density. This approach might thus serve as an example of how the present KMC results are applicable to explain the formation of initial pattern of void volume in solids. Examples include the corrosion of steel (Sun et al., 2015), the formation of secondary porosity due to contrasting defect density pattern in feldspar grains and cements (González-Acebrón et al., 2012; Götze et al., 2000), and the dissolution in battery electrolyte (Steiger et al., 2014). For such systems, we expect the existence of concurrent mechanisms that affect surface reactivity. Such mechanisms include passivation processes during mineral surface reactions due to the formation of altered surface layers (e.g., Daval et al., 2011; Wild et al., 2016).

5 Conclusions

The analysis of Kinetic Monte Carlo simulation results by employing the rate spectra concept provides new insight into the reactivity of crystalline material. The combination of new results about the reduction in reactivity of highly-reactive crystal domains with the quantitative concept of rate spectra may serve as a base for the development of a powerful tool to predict the reactivity of complex crystalline materials. In detail we conclude: The reactivity of a crystalline system can be governed by its reaction history. The dissolution of low-reactivity domains within crystalline matter defines the subsequent reactivity. Crystal domains with high defect densities inherit a lower reactivity close to reacting crystal domains with lower defect densities. Such a mechanism contributes to the explanation of the reduction in surface reactivity of polycrystalline materials. Our results provide a quantitative background to answer questions related to corrosion and dissolution in the material and earth sciences, such as the predetermination of void volume formation with consequences for permeability evolution, as well as for radioactive waste management problems that involve materials with contrasting defect densities.

Acknowledgements

We gratefully acknowledge financial support by the German Research Foundation, DFG grant #Fi1212-7 as well as by the Federal Highway Authority (grant # DTFH61-11-R-00027) and by the Global Climate and Energy Project (GCEP grant 25580430-48513-A). We thank Helge Hellevang and an anonymous reviewer for helpful and constructive comments that clearly improved the manuscript.

References

Anbeek, C., 1992. Surface-Roughness of Minerals and Implications for Dissolution Studies. Geochimica et Cosmochimica Acta 56, 1461-1469.

Anbeek, C., Vanbreemen, N., Meijer, E.L., Vanderplas, L., 1994. The Dissolution of Naturally Weathered Feldspar and Quartz. Geochimica et Cosmochimica Acta 58, 4601-4613.

Anovitz, L.M., Cole, D.R., 2015. Characterization and analysis of porosity and pore structures. Reviews in Mineralogy and Geochemistry 80, 61-164.

Blum, A.E., Lasaga, A.C., 1987. Monte Carlo simulations of surface reaction rate laws., in: Stumm, W. (Ed.), Aquatic Surface Chemistry: Chemical Processes at the ParticleWater Interface. John Wiley and Sons, Inc., pp. 255–292.

Bortz, A.B., Kalos, M.H., Lebowitz, J.L., 1975. A new algorithm for Monte Carlo simulation of Ising spin systems. Journal of Computational Physics 17, 10-18.
Briese, L., Arvidson, R.S., Luttge, A., 2017. The effect of crystal size variation on the rate of dissolution – A kinetic Monte Carlo study. Geochimica et Cosmochimica Acta 212, 167-175.
Burton, W.K., Cabrera, N., Frank, F.C., 1951. The Growth of Crystals and the Equilibrium Structure of Their Surfaces. Philosophical Transactions of the Royal Society of London Series a-Mathematical and Physical Sciences 243, 299-358.
Cama, J., Zhang, L., Soler, J.M., De Giudici, G., Arvidson, R.S., Luttge, A., 2010. Fluorite dissolution at acidic pH: In situ AFM and ex situ VSI experiments and Monte Carlo simulations. Geochimica et Cosmochimica Acta 74, 4298-4311.
Casey, W.H., Carr, M.J., Graham, R.A., 1988. Crystal Defects and the Dissolution Kinetics of Rutile. Geochimica et Cosmochimica Acta 52, 1545-1556.
Chen, L., Kang, Q., Carey, B., Tao, W.-Q., 2014. Pore-scale study of diffusion–reaction processes involving dissolution and precipitation using the lattice Boltzmann method. International Journal of Heat and Mass Transfer 75, 483-496.
Cheng, V.K.W., 1993. A Monte Carlo study of moving steps during crystal growth and dissolution. Journal of Crystal Growth 134, 369-376.
Daval, D., Hellmann, R., Saldi, G.D., Wirth, R., Knauss, K.G., 2013. Linking nm-scale Measurements of the Anisotropy of Silicate Surface Reactivity to Macroscopic Dissolution Rate Laws: New Insights Based on Diopside. Geochimica et Cosmochimica Acta 107, 121-134.
Daval, D., Sissmann, O., Menguy, N., Saldi, G.D., Guyot, F., Martinez, I., Corvisier, J., Garcia, B., Machouk, I., Knauss, K.G., R., H., 2011. Influence of amorphous silica layer formation on the dissolution rate of olivine at 90 °C and elevated pCO2. Chemical Geology 284, 193-209.
Dele-Afolabi, T.T., Hanim, M.A.A., Norkhairunnisa, M., Sobri, S., Calin, R., Investigating the effect of porosity level and pore former type on the mechanical and corrosion resistance properties of agro-waste shaped porous alumina ceramics. Ceramics International.
Dillinger, A., Ricard, L.P., Huddlestone-Holmes, C., Esteban, L., 2014. Impact of Diagenesis on Reservoir Quality in a Sedimentary Geothermal Play: a case study in the Cooper Basin, South Australia. Basin Research, 1-21.
Dong, Y., Lin, B., Zhou, J.-e., Zhang, X., Ling, Y., Liu, X., Meng, G., Hampshire, S., 2011. Corrosion resistance characterization of porous alumina membrane supports. Materials Characterization 62, 409-418.
Dove, P.M., Han, N.Z., De Yoreo, J.J., 2005. Mechanisms of classical crystal growth theory explain quartz and silicate dissolution behavior. Proceedings of the National Academy of Sciences of the United States of America 102, 15357-15362.
Fischer, C., Arvidson, R.S., Luttge, A., 2012. How predictable are dissolution rates of crystalline material? Geochimica et Cosmochimica Acta 98, 177-185.
Fischer, C., Kurganskaya, I., Schäfer, T., Luttge, A., 2014. Variability of Crystal Surface Reactivity: What do we know? (Review Article). Applied Geochemistry 43, 132-157.
Fischer, C., Luttge, A., 2017. Beyond the conventional understanding of water–rock reactivity. Earth and Planetary Science Letters 457, 100-105.
Fischer, C., Luttge, A., 2018. Pulsating dissolution of crystalline matter. PNAS in press.
Gao, J., Xing, H., Tian, Z., Pearce, J.K., Sedek, M., Golding, S.D., Rudolph, V., 2017. Reactive transport in porous media for CO2 sequestration: Pore scale modeling using the lattice Boltzmann method. Computers & Geosciences 98, 9-20.
González-Acebrón, L., Götze, J., Barca, D., Arribas, J., Mas, R., Pérez-Garrido, C., 2012. Diagenetic albitization in the Tera Group, Cameros Basin (NE Spain) recorded by trace elements and spectral cathodoluminescence. Chemical Geology 312–313, 148-162.

Götze, J., Krbetschek, M., Habermann, D., Wolf, D., 2000. High-Resolution Cathodoluminescence Studies of Feldspar Minerals, in: Pagel, M., Barbin, V., Blanc, P., Ohnenstetter, D. (Eds.), Cathodoluminescence in Geosciences. Springer Berlin Heidelberg, pp. 245-270.
Hellevang, H., Pham, V.T.H., Aagaard, P., 2013. Kinetic modelling of CO2–water–rock interactions. International Journal of Greenhouse Gas Control 15, 3-15.
Hiemstra, T., van Riemsdijk, W.H., 1999. Effect of different crystal faces on experimental interaction force and aggregation of hematite. Langmuir 15, 8045-8051.
Horlait, D., Claparede, L., Tocino, F., Clavier, N., Ravaux, J., Szenknect, S., Podor, R., Dacheux, N., 2014. Environmental SEM Monitoring of Ce 1− x Ln x O 2− x/2 mixed-oxide Microstructural Evolution during Dissolution. Journal of Materials Chemistry A 2, 5193-5203.
Iliev, O., Lakdawala, Z., Leonard, K., Vutov, Y., 2015. On pore--scale modeling and simulation of reactive transport in 3D geometries. arXiv preprint arXiv:1507.01894.
Kerisit, S., Rosso, K.M., Cannon, B.D., 2008. Kinetic Monte Carlo model of scintillation mechanisms in CsI and CsI(Tl). Ieee Transactions on Nuclear Science 55, 1251-1258.
Kim, J.-S., Kwon, S.-K., Sanchez, M., Cho, G.-C., 2011. Geological storage of high level nuclear waste. KSCE Journal of Civil Engineering 15, 721-737.
Kossel, W., 1927. Zur Theorie des Kristallwachstums. Nachrichten von der Gesellschaft der Wissenschaften zu Göttingen, Mathematisch-Physikalische Klasse 1927, 135-143.
Kurganskaya, I., Luttge, A., 2016. Kinetic Monte Carlo Approach To Study Carbonate Dissolution. The Journal of Physical Chemistry C 120, 6482-6492.
Lasaga, A.C., Blum, A.E., 1986. Surface chemistry, etch pits and mineral-water reactions. Geochimica et Cosmochimica Acta 50, 2363-2379.
Lasaga, A.C., Luttge, A., 2001. Variation of Crystal Dissolution Rate Based on a Dissolution Stepwave Model. Science 291, 2400-2404.
Lasaga, A.C., Luttge, A., 2004. Mineralogical approaches to fundamental crystal dissolution kinetics. American Mineralogist 89, 527-540.
Liu, Y., Lopes, P.P., Cha, W., Harder, R., Maser, J., Maxey, E., Highland, M.J., Markovic, N.M., Hruszkewycz, S.O., Stephenson, G.B., You, H., Ulvestad, A., 2017. Stability Limits and Defect Dynamics in Ag Nanoparticles Probed by Bragg Coherent Diffractive Imaging. Nano Letters 17, 1595-1601.
Liu, Y., Luo, Y., Elzatahry, A.A., Luo, W., Che, R., Fan, J., Lan, K., Al-Enizi, A.M., Sun, Z., Li, B., Liu, Z., Shen, D., Ling, Y., Wang, C., Wang, J., Gao, W., Yao, C., Yuan, K., Peng, H., Tang, Y., Deng, Y., Zheng, G., Zhou, G., Zhao, D., 2015. Mesoporous TiO2 Mesocrystals: Remarkable Defects-Induced Crystallite-Interface Reactivity and Their in Situ Conversion to Single Crystals. ACS Central Science 1, 400-408.
Luttge, A., 2005. Etch pit coalescence, surface area, and overall mineral dissolution rates. American Mineralogist 90, 1776-1783.
Luttge, A., Arvidson, R.S., Fischer, C., 2013. A Stochastic Treatment of Crystal Dissolution Kinetics. Elements 9, 183-188.
MacInnis, I.N., Brantley, S.L., 1993. Development of Etch Pit Size Distributions on Dissolving Minerals. Chemical Geology 105, 31-49.
Meakin, P., Rosso, K.M., 2008. Simple kinetic Monte Carlo models for dissolution pitting induced by crystal defects. Journal of Chemical Physics 129.
Michaelis, M., Fischer, C., Colombi Ciacchi, L., Luttge, A., 2017. Variability of Zinc Oxide Dissolution Rates. Environmental Science & Technology 51, 4297-4305.
Monger, H.C., Kraimer, R.A., Khresat, S., Cole, D.R., Wang, X., Wang, J., 2015. Sequestration of inorganic carbon in soil and groundwater. Geology 43, 375-378.

Mostaghimi, P., Liu, M., Arns, C.H., 2016. Numerical Simulation of Reactive Transport on Micro-CT Images. Mathematical Geosciences, 1-21.
Pelmenschikov, A., Leszczynski, J., Pettersson, L.G.M., 2001. Mechanism of Dissolution of Neutral Silica Surfaces: Including Effect of Self-Healing. The Journal of Physical Chemistry A 105, 9528-9532.
Peruffo, M., Mbogoro, M.M., Edwards, M.A., Unwin, P.R., 2013. Holistic approach to dissolution kinetics: linking direction-specific microscopic fluxes, local mass transport effects and global macroscopic rates from gypsum etch pit analysis. Physical Chemistry Chemical Physics 15, 1956-1965.
Petrik, M., Harbrecht, B., 2013. Dissolution Kinetics of Nanocrystals. ChemPhysChem 14, 2403-2406.
Renner, F.U., Stierle, A., Dosch, H., Kolb, D.M., Lee, T.L., Zegenhagen, J., 2006. Initial corrosion observed on the atomic scale. Nature 439, 707-710.
Saldi, G.D., Voltolini, M., Knauss, K.G., 2017. Effects of surface orientation, fluid chemistry and mechanical polishing on the variability of dolomite dissolution rates. Geochimica et Cosmochimica Acta 206, 94-111.
Steefel, C.I., Beckingham, L.E., Landrot, G., 2015. Micro-continuum approaches for modeling pore-scale geochemical processes. Reviews in Mineralogy and Geochemistry 80, 217-246.
Steiger, J., Kramer, D., Mönig, R., 2014. Microscopic observations of the formation, growth and shrinkage of lithium moss during electrodeposition and dissolution. Electrochimica Acta 136, 529-536.
Stranski, I.N., 1928. On the theory of crystal accretion. Zeitschrift Fur Physikalische Chemie--Stochiometrie Und Verwandtschaftslehre 136, 259-278.
Sun, G., Zhou, R., Lu, J., Mazumder, J., 2015. Evaluation of defect density, microstructure, residual stress, elastic modulus, hardness and strength of laser-deposited AISI 4340 steel. Acta Materialia 84, 172-189.
Taleb, A., Stafiej, J., 2011. Numerical simulation of the effect of grain size on corrosion processes: Surface roughness oscillation and cluster detachment. Corrosion Science 53, 2508-2513.
Tang, R.K., Henneman, Z.J., Nancollas, G.H., 2003. Constant composition kinetics study of carbonated apatite dissolution. Journal of Crystal Growth 249, 614-624.
Taylor, T.R., Giles, M.R., Hathon, L.A., Diggs, T.N., Braunsdorf, N.R., Birbiglia, G.V., Kittridge, M.G., Macaulay, C.I., Espejo, I.S., 2010. Sandstone diagenesis and reservoir quality prediction: Models, myths, and reality. AAPG Bulletin 94, 1093-1132.
Thomas, T.R., 1999. Rough Surfaces. Imperial College Press, London.
Walrafen, G.E., 1972. Raman and Infrared Spectral Investigations of Water Structure, in: Franks, F. (Ed.), Water, A Comprehensive Treatise, Vol. 1. The Physics and Physical Chemistry of Water. Plenum, New York.
Wild, B., Daval, D., Guyot, F., Knauss, K.G., Pollet-Villard, M., Imfeld, G., 2016. pH-dependent control of feldspar dissolution rate by altered surface layers. Chemical Geology 442, 148-159.
Xu, G., Chen, Z., Zhang, X., Cui, H., Zhang, Z., Zhan, X., 2016. Preparation of porous Al2TiO5-Mullite ceramic by starch consolidation casting and its corrosion resistance characterization. Ceramics International 42, 14107-14112.
Yang, F., Hingerl, F.F., Xiao, X., Liu, Y., Wu, Z., Benson, S.M., Toney, M.F., 2015. Extraction of pore-morphology and capillary pressure curves of porous media from synchrotron-based tomography data. Sci. Rep. 5.